Clays and Clay Minerals, Vol. 50, No. 1, 70–81, 2002.

CRYSTAL CHEMISTRY OF Fe-SUDOITES FROM URANIUM DEPOSITS IN THE ATHABASCA BASIN (SASKATCHEWAN, CANADA)

VALÉRIE BILLAULT*, DANIEL BEAUFORT, PATRICIA PATRIER AND SABINE PETIT

Laboratoire Hydr'ASA, UMR 6532 CNRS, Université de Poitiers, 40 avenue du Recteur Pineau, 86022 Poitiers Cedex, France

Abstract—Sudoites exhibit different crystal-chemical and textural properties which may be related to the structural and valence state of Fe. Mössbauer spectroscopic analysis shows that all Fe previously analyzed using a microprobe (from 1 wt.% to 7.2 wt.% total Fe as Fe_2O_3) is structural and occurs in both oxidation states (40% Fe^{2+} and ~60% Fe^{3+}). Electron microprobe analyses from ~200 sudoites indicate that Fe occurs in both octahedral sheets according to three main types of substitution: Fe^{3+} = octahedral Al; Fe^{2+} = Mg; and Fe^{3+} + Fe^{2+}+ □ = 3Mg. Decreasing tetrahedral substitution balances Fe^{3+} substitution in the trioctahedral sheet. Increasing octahedral Fe results in a more dioctahedral character of sudoite.

X-ray diffraction (XRD), Fourier transform infrared (FTIR) spectroscopy, differential thermal analysis (DTA) and scanning electron microscope-transmission electron microscope (SEM-TEM) analyses showed that increasing octahedral Fe is associated with decreased stacking order and thermal stability due to the greater number of defects. In addition, with increasing octahedral Fe in sudoite, particles became smaller and more anhedral and consequently less stable with increasing Fe content. These structural and textural variations are interpreted as a result of the distortion of the sudoite structure by substitutions of Fe^{3+} with larger ionic radii for Al and Mg octahedral cations and by the formation of octahedral vacancies.

Key Words—Crystal Chemistry, Di-Trioctahedral Chlorite, Fe-Rich Sudoite, Unconformity-Related Uranium Deposits.

INTRODUCTION

Sudoite is a di-trioctahedral Li-free chlorite with a dioctahedral sheet in the 2:1 layer and a trioctahedral interlayer sheet (Bailey, 1980). This type of Al-Mg chlorite usually occurs as a fine-grained clay in various geological environments: sedimentary (Schultz, 1963; Daniels and Altaner, 1990); low-grade metamorphic (Fransolet and Bourguignon, 1978); and hydrothermal alteration associated with ore deposits (Bailey and Tyler 1960; Hayashi and Oinuma, 1964; Sudo and Sato, 1966).

X-ray diffraction patterns of sudoite (Eggleston and Bailey, 1967; Bailey and Lister, 1989) differ from those of other chlorites by a particularly intense *d*(003) reflection (4.76 Å) and a *d*(06.33) reflection (1.50 to 1.51 Å) at an intermediate position between those of dioctahedral (1.49–1.50 Å) and trioctahedral (1.53–1.55 Å) chlorites. Sudoite has been interpreted as the *IIb* structural type (see review in Bailey, 1980).

The ideal structural formula of sudoite is $(Al_3Mg_2)(Si_3Al)O_{10}(OH)_8$, though several studies have indicated that the structural formula of natural sudoites may differ significantly from this ideal formula in the following way (Bailey and Lister, 1989): variation in tetrahedral Al between 0.4 and 1.1 atoms per 4 tetrahedral sites; variation in octahedral Al between 2.5 and 3.4 atoms; variation in octahedral Mg between 1.2 and 2.5 atoms for 5 octahedral sites; variation in the Al/Mg ratio between 1.8 and 2.4. Moreover, small amounts of Fe ranging from 0.3 to 7% of total Fe (*i.e.* FeO + Fe_2O_3) have been measured in natural sudoite (Hayashi and Oinuma, 1964; Kramm, 1980; Fransolet and Bourguignon, 1978; Daniels and Altaner, 1990). In the sudoite structure, the structural Fe has been considered to be in two oxidation states and Sudo and Sato (1966) have suggested the following structural formula for this di-trioctahedral chlorite: $(Al,Fe^{3+})_{4-y}(Mg,Fe^{2+})_{(x/2)+(3y/2)}(Si_{4-x}Al_x)O_{10}(OH)_8$. However, no subsequent investigations explored the role of Fe in the relative stability of sudoite in geological systems.

Large amounts of sudoite have been commonly observed in the clay alteration halos associated with unconformity-related uranium deposits (URUD) (Iida, 1993; Percival and Kodama, 1989). The majority of the Canadian URUD occur in the Athabasca basin (Figure 1). This basin consists of a sequence of middle Proterozoic sandstones unconformably overlying Archean basement (high-grade metamorphic and igneous rocks). Sudoite crystallizations consist of pore-filling in sandstones whereas they are mainly fracture-controlled in the basement. The origin of sudoite in these rocks is still poorly understood. Sudoite is thought to be a hydrothermal alteration product of the interaction of oxidizing and U-rich basinal brines with the different sedimentary rocks encountered above and below the unconformity (Fayek and Kyzer, 1999). Large amounts of sudoite were deposited with uraninite in zones where these oxidizing brines mixed with reducing fluids released from the fractured basement. The temperature of crystallization of these was estimated near 200°C on the basis of isotope composition of associated silicate

* E-mail address of corresponding author:
valerie.billault@hydr asa.univ-poitiers.fr

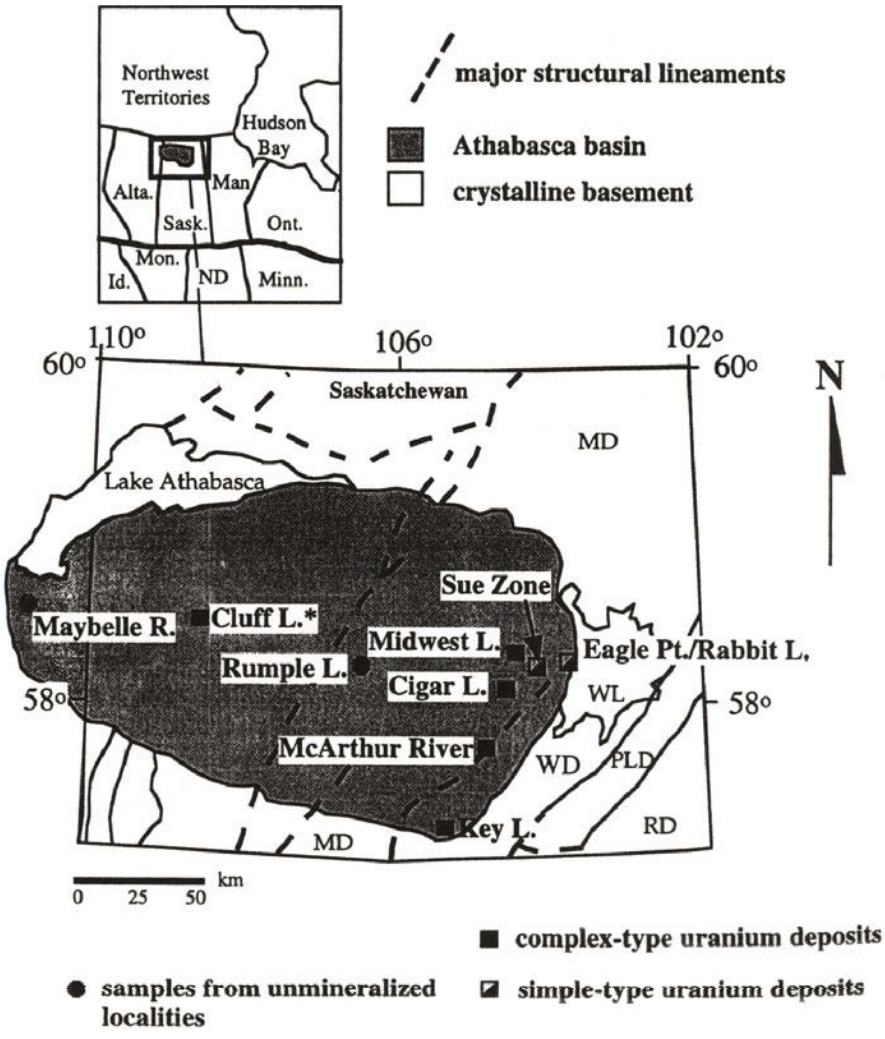

Figure 1. Map of sample localities.

minerals and fluid inclusion microthermometry (Kotzer and Kyser, 1995; Pagel *et al.*, 1980).

The present study focuses on the crystal-chemical and textural properties of three specimens of sudoite from the alteration halo associated with the McArthur River uranium deposit and the Mullins-Johnston prospect. These specimens of sudoites have been chosen because they are representative of the widest variation in Fe content ever reported in sudoite prior to this study (*i.e.* total Fe as Fe_2O_3 ranging from <1% to >7%).

MATERIALS AND METHODS

The samples MR1 and MR2 are from an exploration drill core (MJ03) located in the Mullins-Johnston prospect (West of Cigar Lake, Saskatchewan, Canada). They were collected in the hydrothermally altered sandstones overlying the unconformity in a non-mineralized area. Sample MR11 is from the McArthur River Uranium deposit (Saskatchewan, Canada) and was collected in the underlying metamorphic basement in the mineralized zone. Table 1 summarizes lithological, mineralogical and Fe content data. Both sudoite and illite crystallized as pore fillings in sandstones (samples MR1 and MR2) and fillings in basement fractures (sample MR11). Traces of kaolinites were observed in sample MR1; they correspond to relicts of a general diagenetic process which affects all the sandstone formation of the Athabasca basin prior the hydrothermal occurrences of illite and sudoite. In sample MR11, sudoite and minor trioctahedral chlorite were developed in the fractures of the metamorphic basement.

Clay minerals were extracted by sedimentation after manual grinding of core samples and dispersion of particles in distilled water. Concentrates of sudoite were obtained from the preceding extraction using a method of heavy liquid separation in Na polytungstate (Cassagnabère, 1998). The XRD traces were obtained using a Siemens D500 diffractometer (40 kV, 30 mA) equipped with a Cu target (λ = 1.5406 Å) and Ni filter.

https://doi.org/10.1346/000986002761002847 Published online by Cambridge University Press

The usual step size was 0.025°2θ and counting time was 3 s for all patterns which included air-dried and ethylene glycol-saturated oriented mounts and randomly oriented powders. The methods used to prepare oriented mounts (Millipore filter transfer) and randomly oriented powders are described by Moore and Reynolds (1989). A SOCABIM system (DACO-MP acquisition device) was used for numerical data acquisition and pattern processing which included background stripping and indexing of diffraction peaks. The number of coherently stacked layers was determined by comparing observed XRD patterns with those calculated using the NEWMOD program (Reynolds, 1985). The parameters used for NEWMOD calculations are: Reichweite 0, Söller slits of 6.6° and 2°, divergence slit 1°, *d*(001) chlorite 14.2 Å, goniometer radius 20 cm, sample length 4.5 cm, mass absorption coefficient (mustar) 45, and orientation function (sigma star) 12.

Scanning electron microscope observations on small and freshly fractured core samples coated with gold were made using a JEOL JSM 6400 equipped with a KEVEX energy dispersive spectrometer. The analytical conditions were: accelerating voltage of 15 kV and 100 s counting time.

Transmission electron microscope examination of the particles was performed on a Cu grid covered with a carbon membrane. Semi-quantitative chemical analyses of individual particles were performed using a Philips CM120 transmission electron microscope by means of X-ray analysis using an energy dispersive system associated with a scanning transmission electron microscope (STEM) and a standardless procedure (EDAX).

Chemical analyses of sudoites were obtained on thin-sections using a CAMECA SX50 electron microprobe equipped with wavelength-dispersive spectrometers. The system was calibrated using synthetic and natural oxides and silicates. Corrections were made with a ZAF program. The analytical conditions were: beam current of 4 nA, accelerating voltage of 15 kV, 10 s counting time and a 4 μm spot size. The relative error for the major elements was 1%. Due to the very small size of the sudoite particles and their close association with illite particles, most of the microprobe analyses of sudoites involved small amounts of illite impurities (from 0 to 15%). The structural formulae of the sudoites analyzed in these particles were corrected with respect to the chemical elements corresponding to illite impurities (calculated on the basis of the K content of the sudoite-illite mixture and the structural formula of pure illites measured in each sample).

Infrared spectra were recorded over the range 4000–400 cm^{-1} on a Nicolet 510 FTIR spectrophotometer using pressed disks containing an homogeneous mixture of 3 mg of sudoite and 300 mg of KBr. The spectrometer was continuously purged with dry air during the scanning of the transmission spectra. These disks were placed in a drying oven at 110°C for 12 h before IR analysis.

The Mössbauer spectra were recorded over the range −4.66 to +4.66 mm/s with a spectrometer using a ^{57}Co source (in Rh) of 1.85 Gbq, a Wisel MS1 vibrator, and an γHICI-SEPH detector. They were acquired from finely ground powders at room temperature. Deconvolution of the resulting spectrum was performed on the basis of the least-squares adjustment method involving Lorentzian peak shapes. Isomer shifts were calculated *vs.* Fe metal.

Differential thermal analysis curves were acquired between 20 and 1100°C at a heating rate of 10°C/min with a NETZSCH 409 EP thermal analyser.

RESULTS

Microprobe analysis

Approximately 200 microprobe analyses were collected and Table 2 presents representative analyses of sudoite from the three samples. Concurrently, semi-quantitative chemical analyses were performed at the particle scale using AEM analysis in order to ensure the homogeneity of the particle chemistry. Some variations exhibited by K_2O and CaO due to illite and Ca phosphate impurities, respectively, were observed. Apart from that, the sudoite compositions are nearly constant at the scale of each sample. The three sudoite samples analyzed have a nearly constant amount of SiO_2 but more variable amounts of Al_2O_3 and MgO which decrease as total Fe increases.

Petrographic data and morphology of sudoite

Under plane-polarized light, sudoite appears in samples as a light gray polycrystalline matrix, the individual crystals of which cannot be distinguished. The SEM observations at higher magnification indicate significant variations in the size and morphology of the sudoite particles according to the studied sample (Figure 2). Pore-filling sudoites with low total Fe

Table 1. Lithological and mineralogical characteristics of the core samples from Mullins-Johnston prospect (MR1 and MR2) and from McArthur River uranium deposit (MR11).

Sample	Lithology	Clay assemblage	Total Fe in sudoite (%)
MR1	altered sandstone	sudoite + illite + kaol.	<1.0
MR2	altered sandstone	sudoite + illite	3.7
MR11	altered mica-schist	sudoite + illite + trichl.	7.2

kaol. = kaolinite, trichl. = trioctahedral chlorite.

https://doi.org/10.1346/000986002761002847 Published online by Cambridge University Press

Table 2. Representative compositions of sudoite analyzed by electron microprobe.

Sample	SiO_2	Al_2O_3	MgO	*Fe_2O_3	MnO	CaO	Na_2O	K_2O	Sum
MR1	37.02	35.61	11.07	0.89	0.07	0.02	0.08	1.10	85.86
MR2	36.70	33.04	11.04	3.74	0	0.07	0.09	0.49	85.17
MR11	36.81	30.58	8.13	7.25	0.11	0.33	0.05	0.76	84.02

* Total Fe is considered arbitrarily as Fe_2O_3. Analyses are not corrected for minor inclusions of illite and Ca phosphates.

content (sample MR1) show a boxwork pattern oriented perpendicular to the wall-rock surface. At higher magnification the boxwork appears to be composed of folded packets of subhedral platy crystals whose average size reaches 2–3 μm. Sudoites with higher total Fe content (MR11) developed in the fractures differ from the previous one by a smaller particle size (1 μm in average diameter), an orientation parallel to the wall-rock surface and a rather anhedral flaky morphology when observed at higher magnification. This particular texture is probably related to the previous textural properties of the altered metamorphic basement. The textural properties of sudoite with intermediate total Fe content (sample MR2) are intermediate between MR1 and MR11 (intermediate arrangement between boxwork and parallel patterns).

X-ray diffraction data

The XRD patterns of oriented preparations (2 μm size-fraction) of sudoites analyzed in the air-dried state (Figure 3a) exhibit characteristic 00*l* reflections at 14.20, 7.165, 4.75 and 3.54 Å with a particularly intense 003 reflection. None of these 00*l* reflections is affected by ethylene glycol solvation. All of the XRD patterns of randomly oriented powders (Figure 3b) show *hkl* reflections of the *IIb* polytype of sudoite (JCPDS data file n°19-0751), though the intensity and the peak widths of the XRD reflections and the position of their 06.33 reflection vary systematically as the total Fe content of sudoites increases (Table 3). These variations may be summarized as follows: (1) the intensity of the 003 reflections decrease by a factor of 5; (2) the FWHM of 001 and 002 reflections increases by 50%; (3) the 001/003 intensity ratios increase from 0.27 to 0.5; (4) the position of the 06.33 reflection shifts from 1.50 to 1.511 Å.

The XRD patterns showing 00*l* reflections with FWHM values similar to those measured in our samples have been simulated (NEWMOD computer program, Reynolds, 1985) using a number of coherently diffracting layers (*N*) which decreases from 16 in Fe-poor sudoites to 12 in Fe-rich sudoites.

Infrared analysis

Figure 4 shows the normalized FTIR spectra in the OH-stretching region (3700 and 3300 cm^{-1}) and the OH-bending region (1100 and 400 cm^{-1}) for the sudoites analyzed. The IR bands of kaolinite impurities (3698, 3616 and 920 cm^{-1}) are identified in the spectrum of sample MR1.

The IR spectrum of the most Fe-rich sudoite (MR11) differs from the others by a general broadening and decrease in the intensity of IR bands that often inhibits the distinction of neighboring IR bands. This phenomenon indicates a high density of defects in sudoite.

Table 4 summarizes the IR absorption bands of different sudoites containing variable amounts of total Fe ranging from 2.5 to 5.5% (Hayashi and Oinuma, 1965; Fransolet and Bourguignon, 1978; Kawano and Tomita, 1991) as well as the samples studied in this paper. Most of the absorption bands observed in our samples are in common with those reported in the literature. However, the absorption bands located at 830, 620 and 560 cm^{-1} due to the (SiAl)OOH bond (Farmer, 1974), and to octahedral Mg and octahedral Al (Hayashi and Oinuma, 1967), respectively, cannot be identified

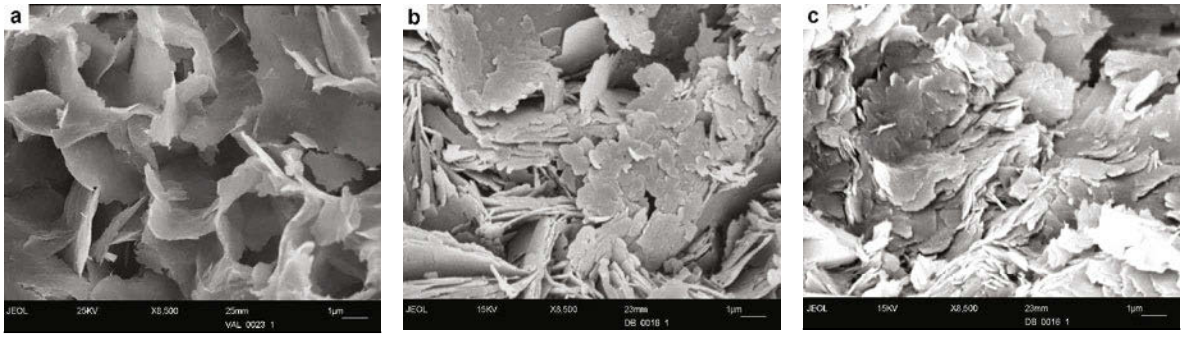

Figure 2. Scanning electron photomicrographs of sudoite: (a) from sample MR1 showing a boxwork pattern oriented perpendicular to the wall-rock surface; (b) from sample MR2 representing an intermediate arrangement between boxwork and parallel patterns; and (c) from sample MR11 presenting smaller particle size and an orientation parallel to the wall-rock surface.

https://doi.org/10.1346/000986002761002847 Published online by Cambridge University Press

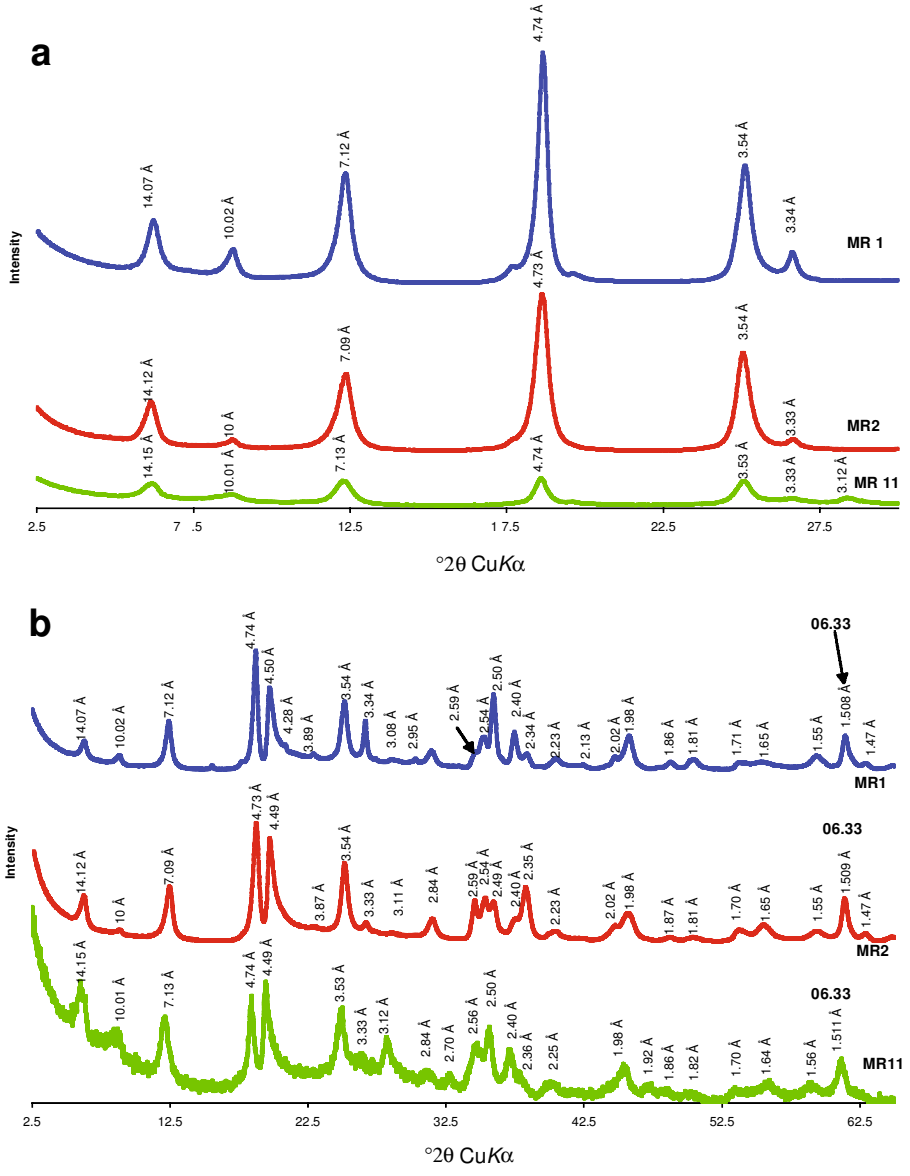

Figure 3. (a) XRD patterns of the three oriented air-dried samples; and (b) XRD patterns of randomly oriented powders of sudoite samples normalized to the 003 reflection.

clearly in the spectrum of Fe-rich sudoite (sample MR11). This is probably due to the weakening and broadening of these absorption bands resulting from the high density of defects contained in these crystals of Fe-rich sudoite.

Thermal behavior

The DTA curves of sudoites analyzed differ according to their Fe content (Figure 5). They show a strong dehydroxylation endothermic peak for which the peak temperature (T_{max}) and asymmetry vary significantly.

Table 3. XRD characteristics and related structural parameters of the analyzed sudoites.

Sample	Total Fe in sudoite	$I_{(003)}$	$I_{(001)}/I_{(003)}$	$FWHM_{(001)}$	$FWHM_{(002)}$	*b* parameter (Å)	*N* (NEWMOD)	*d*(06,33) (Å)
MR1	<1.0%	3200	0.50	0.41	0.46	9.048	16	1.508
MR2	3.7%	2000	0.27	0.47	0.59	9.054	13	1.509
MR11	7.2%	600	0.50	0.60	0.62	9.090	12	1.511

I = intensity (counts/s), FWHM= full width at half maximum intensity, *N* = number of coherently stacking layers.

https://doi.org/10.1346/000986002761002847 Published online by Cambridge University Press

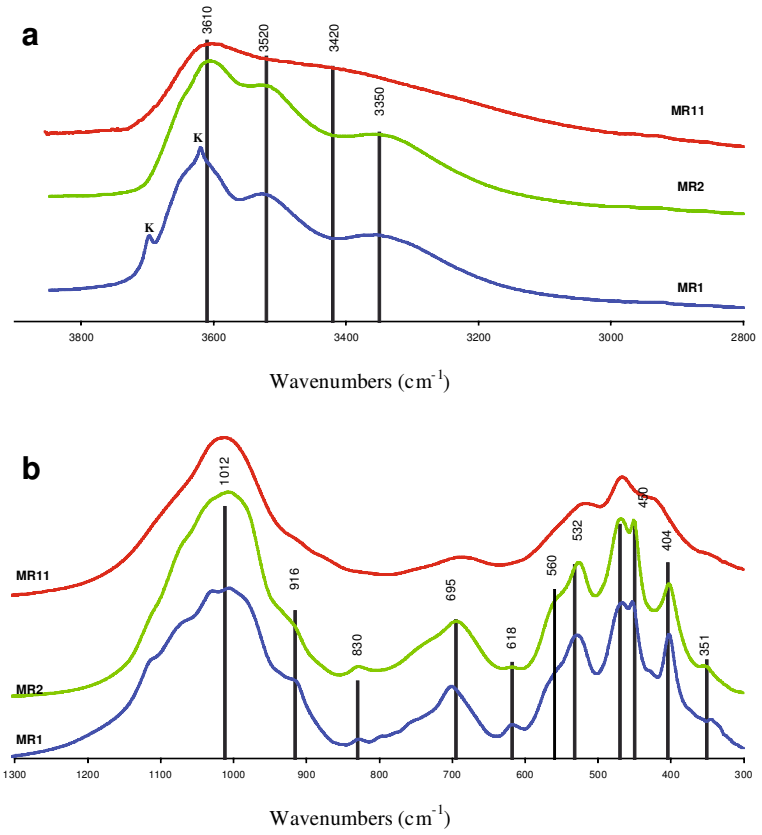

Figure 4. FTIR spectra of sudoite samples: (a) in the OH-stretching vibration zone; (b) in the 1300–300 cm^{-1} zone. K = kaolinite.

The T_{max} values of 578, 568 and 466°C were measured in sudoites containing <1, 3.7 and 7.2% Fe, respectively. All these endothermic peaks are asymmetric towards lower temperatures but the asymmetry is greatest for Fe-rich sudoite. Peak asymmetry of the DTA usually results from particle-size heterogeneity and high defect densities in crystals (Koster van Groos and Guggenheim, 1990). The fact that SEM observations did not reveal any difference in particle size heterogeneity among the studied samples implies that Fe-rich sudoite contains a high density of defects. The DTA curves of samples MR1 and MR2 (containing $\leqslant$3.7% total Fe) show a very weak endothermic peak near 800–850°C which is not perceptible in the case of Fe-rich sudoite (MR11). All the DTA curves show an exothermic peak the T_{max} of which decreases systematically from 914 to 858°C as the total Fe content of sudoite increases.

Mössbauer spectroscopy

Table 5 lists calculated parameters from Mössbauer spectra of the sudoite samples with 3.7 and 7.2% of total Fe. In both cases, no trace of discrete Fe oxides was

Table 4. IR absorption band parameters (cm^{-1}) from sudoite spectra from this work and from the literature. (1) Hayashi and Oinuma (1964); (2) Kawano and Tomita (1991); (3 and 4) Fransolet and Bourguignon (1978).

(1) Kamikita Fe: 5.5%	(2) Makurazaki Fe: 3%	(3) Ottre Fe: 3%	(4) Regne Fe: 2.5%	MR1 Fe: <1%	MR2 Fe: 3.7%	MR11 Fe: 7.2%
3620	3616	3600	3600	3621	3612	3608
3520 and 3340	3510 and 3340	3520 and 3375	3525 and 3400	3526 and 3358	3521 and 3353	3440
1007	998	1000	1000	1020	1020	1020
825	834 sh	830	832	830	831	–
692	699	693	690	707	698	686
–	–	–	–	618 sh	616 sh	–
555	560 sh	550 sh	552 sh	568 sh	566 sh	–
528	530	528	532	532	530	520
475	469 and 454	473 and 453	472 and 453	470 and 450	473 and 453	473 and 425

sh = shoulder

–: no absorption bands located at this wavenumber

https://doi.org/10.1346/000986002761002847 Published online by Cambridge University Press

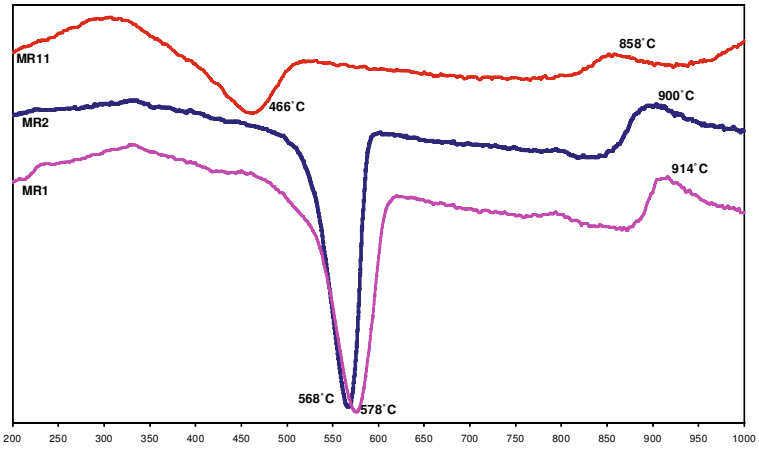

Figure 5. DTA curves from the three samples.

detected and the best fit was obtained with two Fe^{3+} doublets and one Fe^{2+} doublet (Figure 6), each one corresponding to sites of octahedral coordination in chloritic minerals (De Parseval *et al.*, 1991; De Grave *et al.*, 1987; Coey, 1984). The calculated parameters obtained for sample MR2 indicate doublets with isomeric shift (IS) values of 0.25 and 0.25 mm/s and quadrupolar splitting (QS) values of 0.55 and 1.22 mm/s, respectively, in accordance with Fe^{3+} in octahedral coordination. The high QS value (1.22 mm/s) calculated for the latter doublet suggests a distortion of the site (Pal *et al.*, 1992). The doublet with IS value 1.00 mm/s and QS value 2.53 mm/s is compatible with Fe^{2+} in octahedral coordination. The calculated parameters obtained for sample MR11 indicate that octahedral Fe^{3+} is characterized by two doublets with IS values of 0.23 and 0.25 mm/s and QS values of 0.57 and of of 1.04 mm/s, respectively; Fe^{2+} is characterized by a doublet with an IS value of 0.99 mm/s and a QS value of 2.37 mm/s. Our results indicate that both samples of sudoite have similar Fe^{2+}/Fe^{3+} ratios with a predominance of ferric Fe. The Fe^{3+} percentages reach 56 and 60% in sudoites containing 3.7 and 7.2% of total Fe, respectively.

DISCUSSION

Crystal chemistry of sudoites

The textural and crystal-chemical properties of sudoites analyzed vary systematically as a function of their Fe content. Variations in the *b* parameter measured from XRD patterns and computed data from Mössbauer spectra confirm that all the Fe measured by microprobe is structural and located in different octahedral sites of sudoite. The Fe occurs in octahedral sites as Fe^{2+} and Fe^{3+}, the relative proportions of which are 44 and 56% in sudoites containing 3.7% total Fe and 40 and 60%, respectively, in sudoites containing 7.2% total Fe. Sudoite structural formulae have been calculated (Table 6) based on the compositions in Table 2 (corrected for the illite and Ca phosphate impurities identified by AEM analysis) and on the Mössbauer results. These structural formulae are consistent with a di-trioctahedral chlorite structure and coincide with the compositional range of sudoite reported in the literature (Table 7). However, the amount of Fe analysed in sample MR11 is the highest ever reported although analogs of Fe-rich sudoite containing up to 0.63 atoms of Fe^{2+} have been suspected but not characterized (Stanton, 1984).

Table 5. Mössbauer parameters (mm/s) of the Lorentzian doublets after the spectral decomposition of the sudoites sample MR2 and MR11. Δ: quadrupole splitting; δ: isomer shift; Γ: width at half height; θ: amplitude; %: relative area of each doublet.

Sample	Δ	δ	θ	Γ	Oxidation state	Fe coordination	%
MR2	0.549	0.253	0.003	0.35	Fe^{3+}	Octahedral	29.9
	1.222	0.248	0.002	0.6	Fe^{3+}	Octahedral	25.7
	2.528	0.999	0.005	0.35	Fe^{2+}	Octahedral	44.4
MR11	0.576	0.23	0.015	0.422	Fe^{3+}	Octahedral	31.8
	1.044	0.252	0.011	0.544	Fe^{3+}	Octahedral	27.8
	2.372	0.992	0.016	0.529	Fe^{2+}	Octahedral	40.4

https://doi.org/10.1346/000986002761002847 Published online by Cambridge University Press

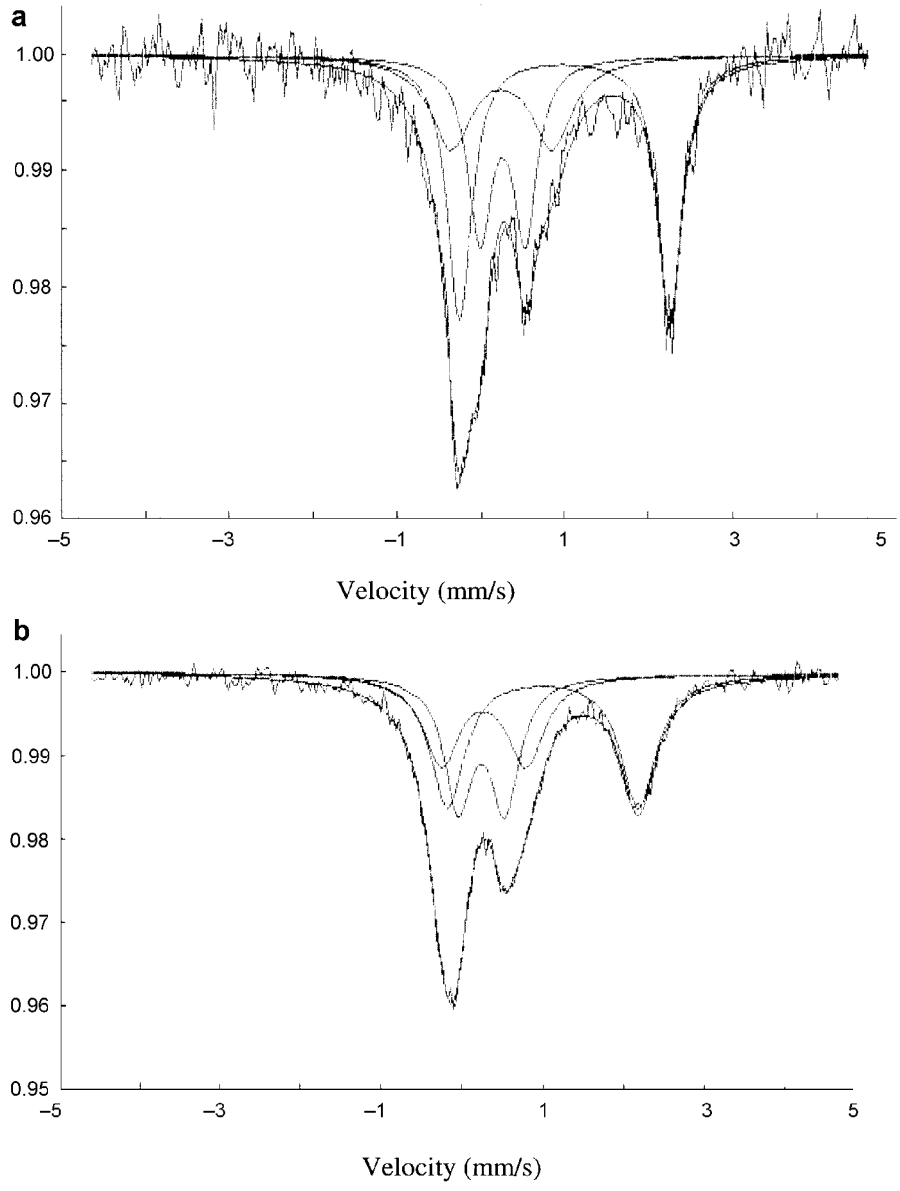

Figure 6. Mössbauer spectra recorded at ambient temperature: (a) sample MR2; and (b) sample MR11. Mössbauer parameters of doublets are given in Table 5.

The structural formulae of sudoite in this study indicate that the changing Fe content is accompanied by significant compositional variations in the octahedral and tetrahedral sheets. An increase in the total Fe content from 0.05 to 0.57 atoms leads to the following: a decrease in tetrahedral charge (from 0.77 to 0.58); a decrease in octahedral Al and Mg (from 3.11 to 2.87 and from 1.65 to 1.24, respectively); and a decrease in octahedral occupancy (from 4.81 to 4.69). The variations described above cannot be explained other than by the

Table 6. Structural formulae of sudoites calculated on the basis of 14 oxygens after corrections for illite and Ca phosphate impurities.

Sample	Si	Al^{IV}	Al^{VI}	Fe^{3+}	Fe^{2+}	Mg	Mn	Oct. Occ.
MR1	3.23	0.77	3.11	0.03	0.02	1.65	0	4.81
MR2	3.32	0.68	2.93	0.15	0.13	1.58	0	4.79
MR11	3.42	0.58	2.87	0.33	0.24	1.24	0.01	4.69

https://doi.org/10.1346/000986002761002847 Published online by Cambridge University Press

Table 7. Structural formulae of sudoites reported in the literature.

	1	2	3	4	5	6	7	8	9	10	11	12	13	14	15	16	17	18
SiO_2	34.36	33.71	33.10	36.07	32.81	33.06	33.83	32.45	31.17	32.46	35.63	39.01	35.67	35.70	32.90	39.25	34.74	33.17
Al_2O_3	38.34	37.95	37.43	32.42	35.71	35.74	31.80	34.88	37.49	35.83	34.87	32.15	37.41	33.77	35.40	32.94	36.69	33.71
TiO_2			0.30		0.18		0.34					0.47	0.19		0.06	0.48		
Fe_2O_3	0.49	2.74	0.87	1.99	2.66	2.74	0.27		1.04		5.01	0.9	0.2	2.81	2.69	2.98		
FeO		2.4			1.07	0.24	0.37	3.48	1.95	2.58	0.43	0.10	0.09	0.35			3.42	7.00
MnO					0.29	0.28		0.41		0.31	0.05		0.02	0.04	0.01			
MgO	10.21	12.08	13.12	15.94	13.54	14.09	18.86	13.56	14.25	13.64	8.63	10.14	11.97	13.26	14.73	9.49	12.92	8.88
CaO	0.07	1.49			0.03		1.8		0.26		1.13	0.54	0.66			0.01		
Li_2O														0.06	0.04	0.02		
Na_2O	0.06		0.15	0.44			0.58				0.24	0.1	0.16		0.01	0.08		
K_2O	0.12		0.29		0.03		0.04				0.46	1.52	0.43			0.17		
Numbers of cations on the basis of $O_{10}(OH)_8$																		
Si	3.12	2.97	3.01	3.24	2.99	3.01	3.04	3.03	2.85	3.01	3.26	3.56	3.18	3.24	3	3.54	3.1	3.21
Al^{IV}	0.88	1.03	0.99	0.76	1.01	0.99	0.96	0.97	1.15	0.99	0.74	0.44	0.82	0.76	1	0.46	0.9	0.79
Tet. Occ.	4	4	4	4	4	4	4	4	4	4	4	4	4	4	4	4	4	4
Al^{VI}	3.29	2.9	3.03	2.67	2.84	2.84	2.4	2.86	2.9	2.92	3.02	3.02	3.11	2.85	2.81	3.04	2.96	3.05
Ti			0.02		0.01		0.03					0.03	0.01			0.03		
Fe^{3+}	0.03	0.18	0.06	0.13	0.18	0.19	0.03		0.07		0.34	0.06	0.01	0.19	0.18	0.2		
Fe^{2+}		0.17			0.08	0.02	0.04	0.27	0.15	0.2	0.04	0.01	0.01	0.03			0.25	0.52
Mn					0.02	0.02		0.03		0.02								
Mg	1.39	1.58	1.78	2.14	1.84	1.91	2.5	1.88	1.95	1.88	1.17	1.37	1.59	1.79	2	1.28	1.73	1.28
Li														0.02				
Oct. Occ.	4.71	4.83	4.89	4.94	4.97	4.98	5	5.04	5.07	5.02	4.57	4.49	4.73	4.88	4.99	4.55	4.94	4.85
Ca		0.14			0.01						0.11	0.05	0.06					
Na	0.11		0.03	0.07								0.02	0.03			0.01		
K	0.01		0.04		0.01							0.18	0.05			0.02		

(1) Sudo and Shimoda (1978)
(2) Alysheva *et al*. (1977)
(3) Kimbara and Nagata (1974)
(4) Alysheva *et al*. (1977)
(5) Kramm (1980)
(6) Fransolet and Bourguignon (1978)
(7) Alysheva *et al*. (1977)
(8) Kramm (1980): all Fe as FeO
(9) Drits and Lazarenko (1967)
(10) Kramm (1980): all Fe as FeO
(11) Hayashi and Oinuma (1964)
(12) Tsukahara (1964)
(13) Sudo and Shimoda (1978)
(14) Anceau (1992)
(15) Lin and Bailey (1985)
(16) Kawano and Tomita (1991)
(17) Daniels and Altaner (1990)
(18) Daniels and Altaner (1990)

substitution of Fe^{3+} for Al in the dioctahedral sheet (Figure 7a) and of Fe^{2+} for Mg in the trioctahedral sheet (Figure 7b) as previously proposed by Sudo and Sato (1966). Indeed, none of the above substitutions balances the overall electrical charge resulting from the observed decrease of the tetrahedral charge with increasing structural Fe. Two types of substitutions may be invoked: Fe^{2+} for octahedral Al and $Fe^{2+} + Fe^{3+} + \square$ for 3Mg (Figure 7c) in octahedral sites. The decrease of octahedral occupancy (from 4.81 to 4.69) measured indicates that the latter type of substitution is the most likely (Figure 7c).

Increasing amounts of octahedral Fe in sudoite also tend to shift the structure of sudoite towards the dioctahedral chlorite end-member and not towards the trioctahedral one as may be expected from its common association with Fe-rich trioctahedral chlorite. Trioctahedral Fe-rich chlorites coexisting with sudoites have been observed in the studied samples and are also reported in other unconformity-related uranium deposits (Pacquet and Weber, 1993; Percival and Kodama, 1989). The relations between sudoites and Fe-rich trioctahedral chlorites are poorly known in these geological environments. However, the deviation of the structural formula

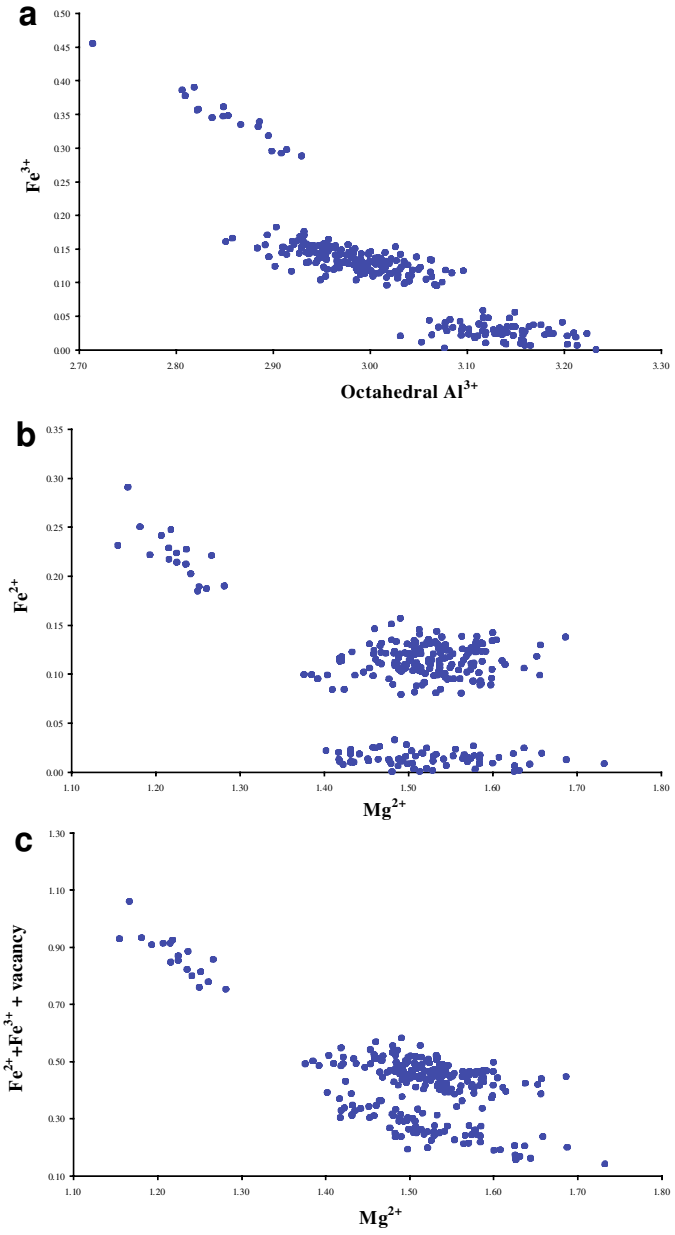

Figure 7. Inter-element correlations between octahedral components of the sudoites: (a) Fe^{3+} *vs.* octahedral Al^{3+}; (b) Fe^{2+} *vs.* Mg^{2+}; and (c) $Fe^{2+} + Fe^{3+}$ + vacancy *vs.* Mg^{2+}.

https://doi.org/10.1346/000986002761002847 Published online by Cambridge University Press

of sudoites towards the dioctahedral chlorite end-member as their Fe content increases argues against intergrowth or solid solution with coexisting Fe-rich chlorite.

Relation between Fe content, structural parameters and particle thickness

Herbillon *et al.* (1976) and Brindley and Kao (1986) studied the effect of Fe content on kaolinite structure. They showed that increasing structural Fe in kaolinite is correlated with a decrease in size and degree of crystallinity. Mestdagh *et al.* (1980) observed that increasing the structural Fe content in natural kaolinites is correlated with an increase of structural defects created by displacement of octahedral vacancy. So, increasing the amount of structural Fe in sudoites seems to have similar consequences to those measured in kaolinite, *i.e.* decreasing particle thickness and increasing structural disorder (Rengasamy *et al.*, 1975; Petit and Decarreau, 1990, among others).

The XRD patterns of sudoites with a total octahedral Fe content ranging from 0.05 to 0.57 atoms per $O_{10}(OH)_8$ indicate that increasing the amount of structural Fe is correlated with decreasing crystallinity (as shown by the weakening and broadening of XRD reflections and the decrease in the number of coherently stacked layers).The FTIR data indicate that structural disorder increases with increasing structural Fe. It should be noted that IR spectra are influenced by the density of defects located in the layers and not by the layer stacking faults as considered by crystallinity. The DTA curves show that the thermal stability of sudoite decreases as the amount of structural Fe increases in response to increasing disorder. All these structural variations can be explained by the distortion of the sudoite structure induced by the various substitutions of Fe (with relatively large ionic radii) for octahedral Al (substitution of Fe^{3+} for Al and Fe^{2+} for Al) and for Mg (substitution of Fe^{2+} for Mg and $Fe^{2+} + Fe^{3+} + \square$ for 3Mg), and by the occurrence of vacancies ($Fe^{2+} + Fe^{3+} + \square$ = 3Mg substitution). Such distortions should disrupt stacking regularity and result in a poorer crystallinity. A decrease in particle size and morphological changes from subhedral to anhedral platy particles were observed as the amount of octahedral Fe increased. This may be interpreted as a result of the increasing structural disorder in sudoites and may account for their relative instability compared to the Al- or Mg-rich sudoite end-members.

ACKNOWLEDGMENTS

The authors thank M. Garais for the DTA analyses, C. Besse for the AEM analyses and COGEMA for kindly providing the samples. Peter Ryan, Peter Schiffman and Stephen P. Altaner are thanked for their careful and constructive reviews.

REFERENCES

Alysheva, E.I., Rusinova, O.V. and Chekvaidze, V.B. (1977) On sudoites from the polymetal deposits of Rydnyy Altai. *Doklady Academii Nauk SSSR*, **236**, 722–724.

Anceau, A. (1992) Sudoite in some Visean (lower Carboniferous) K-bentonites from Belgium. *Clay Minerals*, **27**, 283–292.

Bailey, S.W. (1980) Structure of layer silicates. Pp. 28–39 in: *Crystal Structure of Clay Minerals and their X-ray Identification* (G.W. Brindley and G. Brown, editors). Monograph **5**, Mineralogical Society, London.

Bailey, S.W. and Lister, J.S. (1989) Structures, compositions, and X-ray identification of dioctahedral chlorites. *Clays and Clay Minerals,* **37**, 193–202.

Bailey, S.W. and Tyler, S.A. (1960) Clay minerals associated with the Lake Superior iron ores. *Economic Geology,* **55**, 150–175.

Brindley, G.W. and Kao, C. (1986) Relation between structural disorder and other characteristics of kaolinites and dickites. *Clays and Clay Minerals*, **34**, 239–249.

Cassagnabère, A. (1998) Caractérisation et interprétation de la transition kaolinite-dickite dans les réservoirs à hydrocarbures de Froy et Rind (Mer du Nord, Norvège). Ph.D. thesis, Université de Poitiers, Poitiers, France, 238 pp.

Coey, J.M.D. (1984) Mössbauer spectroscopy of silicate minerals. Pp. 443–509 in: *Mössbauer Spectroscopy Applied to Inorganic Chemistry* (G.J. Long, editor). Plenum Press, New York.

Daniels, E.J. and Altaner S.P. (1990) Clay mineral authigenesis in coal and shale from the Anthracite region, Pennsylvania. *American Mineralogist*, **75**, 825–839.

De Grave, E., Vandenbruwaene, J. and Van Bockstael, M. (1987) ^{57}Fe Mössbauer spectroscopic analysis of chlorite. *Physics and Chemistry of Minerals*, **15**, 173–180.

De Parseval, P., Fournes, L., Fortune, J.P., Moine, B. and Ferret, J. (1991) Distribution du fer dans les chlorites par spectrométrie Mössbauer (^{57}Fe): Fe^{3+} dans les chlorites du gisement de talc-chlorite de Trimouns (Pyrénées, France). *Compte-rendu de l'Académie des Sciences de Paris*, **312**, 1321–1326.

Drits. V.A. and Lazarenko, E.K. (1967) Structural-mineralogical characteristics of donbassites. *Mineral Sbornik, Lvov*, **21**, 40–48.

Eggleston, R.A. and Bailey, S.W.(1967) Structural aspects of dioctahedral chlorite. *American Mineralogist*, **52**, 673–689.

Farmer, V.C. (editor) (1974) The layer silicates. Pp. 331–363 in: *Infrared Spectra of Minerals*. Monograph **4**. Mineralogical Society, London.

Fayek, M. and Kyser, T.K. (1999) Stable isotope geochemistry of uranium deposits. Pp. 181–220 in: *Uranium: Mineralogy, Geochemistry and the Environment* (P.C. Burns and R. Finch, editors). Reviews in Mineralogy, **38**. Mineralogical Society of America, Washington, D.C.

Fransolet, A.M. and Bourguignon, P. (1978) Di/trioctahedral chlorite in quartz veins from the Ardennes, Belgium. *Canadian Mineralogist,* **16**, 365–373.

Hayashi, H. and Oinuma, K. (1964) Aluminian chlorite from Kamikita mine, Japan. *Clay Science*, **2**, 22–30.

Hayashi, H. and Oinuma, K. (1965) Relationship between infrared absorption spectra in the region of 450-900 cm^{-1} and chemical composition of chlorite. *American Mineralogist*, **50**, 476–483.

Hayashi, H. and Oinuma, K. (1967) Si-O absorption band near 1000 cm^{-1} and OH bands of chlorite. *American Mineralogist,* **52**, 1206–1210.

Herbillon, A.J., Mestdagh, M.M., Vielvoye, L. and Derouane, E.G. (1976) Iron in kaolinite with special reference to kaolinite from tropical soils. *Clay Minerals*, **11**, 201–219.

Iida, Y. (1993) Alteration and ore-forming processes of unconformity related uranium deposits. *Resource Geology, Special Issue,* **15**, 299–308.

Kawano, M. and Tomita, K. (1991) Mineralogy and genesis of clays in postmagmatic alteration zones, Makurazaki volacanic area, Kagoshima prefecture, Japan. *Clays and Clay Minerals*, **39**, 597–608.

Kimbara, K. and Nagata, H. (1974) Clay minerals in the core samples of the mineralized zone of Niida, southern part of Odate Akita Prefecture, Japan. *Japanese Association of Mineralogists, Petrologists and Economic Geologists Journal*, **69**, 239–254.

Koster van Groos, A.F. and Guggenheim, S. (1990) High-pressure differential thermal analysis: applications to clay minerals. Pp. 49–94 in: *Thermal Analysis in Clay Science* (J.W. Stucki, D.L. Bish and F.A. Mumpton, editors). CMS Workshop Lectures, **3**. The Clay Minerals Society, Boulder, Colorado., USA.

Kotzer, T.G. and Kyser, T.K. (1995) Petrogenesis of the Proterozoic Athabasca Basin, northern Saskatchewan, Canada, and its relation to diagenesis, hydrothermal uranium mineralization and paleohydrogeology. *Chemical Geology*, **120**, 45–89.

Kramm, U. (1980) Sudoite in low-grade manganese rich-assemblages. *Neues Jahrbuch für Mineralogie, Abhandlungen,* **138**, 1–13.

Lin, C.Y. and Bailey, S.W. (1985) Structural data for sudoite. *Clays and Clay Minerals*, **33**, 410–414.

Mestdagh, M.M., Vielvoye, L. and Herbillon, A.J. (1980) Iron in kaolinite: II. The relationship between kaolinite crystallinity and iron content. *Clay Minerals*, **15**, 1–13.

Moore, D.M. and Reynolds, R.C., Jr. (editors) (1989) Sample preparation techniques for clay minerals. Pp. 179–201 in: *X-ray Diffraction and the Identification and Analysis of Clay Minerals*. Oxford University Press, New York.

Pacquet, A. and Weber, F. (1993) Pétrographie et minéralogie des halos d'altérations autour du gisement de Cigar Lake et leurs relations avec les minéralisations. *Canadian Journal of Earth Sciences,* **30**, 674–688.

Pagel, M., Poty, B. and Sheppard, S.M.F. (1980) Contributions to some Saskatchewan uranium deposits mainly from fluid inclusions and isotopic data. Pp. 639–654 in: *Uranium in Pine Creek Geosyncline* (S. Ferguson and A. Gobely, editors). IAEA, Vienna.

Pal, T., Das, D. and Mitra, S. (1992) ^{57}Fe Mössbauer investigation of naturally oxidised chlorite. *Hyperfine Interactions*, **73**, 313–321.

Percival, J.B. and Kodama, H. (1989) Sudoite from Cigar Lake, Saskatchewan. *Canadian Mineralogist,* **27**, 633–641.

Petit, S. and Decarreau, A. (1990) Hydrothermal (200°C) synthesis and crystal chemistry of iron-rich kaolinites. *Clay Minerals*, **25**, 181–196.

Rengasamy, P. and Krishna Murti, G.S.R. and Sarma, V.A.K. (1975) Isomorphous substitution of iron for aluminum in some soil kaolinites. *Clays and Clay Minerals*, **23**, 211–214.

Reynolds, R.C., Jr. (1985) *NEWMOD: a Computer Program for the calculation of one-dimensional patterns of mixed-layered clays*. R.C. Reynolds, 8 Brook Rd., Hanover, New Hampshire, USA.

Schultz, L.G. (1963) Clay minerals in Triassic rocks of the Colorado Plateau. *US Geological Survey Bulletin,* **1147-C**.

Stanton, R.L. (1984) The direct derivation of cordierite from a clay-chlorite precursor: evidence from the Greco mine, Manitouwadge, Ontario. *Economic Geology*, **79**, 1245–1264.

Sudo, T. and Sato, M. (1966) Dioctahedral chlorite. *Proceedings of the International Clay Conference, Jerusalem,* **1**, 33–39.

Sudo, T. and Shimoda, S. (1978) *Clays and Clay Minerals of Japan*. Developments in Sedimentology, **26**. Elsevier, Amsterdam, 326 pp.

Tsukahara, N. (1964) Dioctahedral chlorite from the Furutobe mine, Akita prefecture, Japan. *Clay Science*, **2**, 56–75.

(*Received 23 October 2000; revised 31 May 2001; Ms. 494; A.E. Stephen Altaner*)